Bulletin of Engineering Geology and the Environment (2020) 79:4411–4427
https://doi.org/10.1007/s10064-020-01805-y

ORIGINAL PAPER

Laboratory characterization of sandy soil water content during drying process using electrical resistivity/resistance method (ERM)

Ni An[1,2] · Chao-Sheng Tang[1] · Qing Cheng[1] · De-Yin Wang[1] · Bin Shi[1]

Received: 16 August 2019 / Accepted: 8 April 2020 / Published online: 9 May 2020

Abstract

Drought-induced evaporation can reduce soil water content and significantly alter soil hydro-mechanical behavior. Understanding the temporal and spatial distribution characteristics of soil water content during evaporation is of great significance for evaluating the encountered geotechnical and geo-environmental problems in arid or semi-arid regions. In this study, an electrical resistivity/resistance method (ERM) with a high spatial resolution of centimeter-level was developed for a small-scale laboratory test and applied to quantitatively characterize the evaporation-induced water content variations along a depth gradient. A total of 8 groups of initially saturated sandy soil columns (84 mm in diameter and 290 mm in height) were prepared, and eight pairs of mini electrodes (3.5 mm in diameter) were installed in each soil sample with a vertical distance of 30 mm. The soil columns were subjected to continuous drying. The changes in soil electrical resistance at different depths were monitored by the electrode couples. The gravimetric water contents at different depths were also measured at the end of drying. It is found that soil water content decreases exponentially with increasing electrical resistance. Based on the obtained data, a calibration relationship between soil gravimetric water content and corrected electrical resistance was well established with consideration of temperature effect. This relationship was validated successfully by the experimental results, indicating the feasibility of the developed ERM to characterize the soil water content dynamics during the drying process. Besides, the drying process with the movement of the evaporation front was discussed. The results of this study demonstrate the good performance of ERM in the estimation of temporal and spatial variations of soil water content and its potential application in arid or semi-arid regions with frequent droughts.

Keywords Soil water evaporation · Soil water content · Electrical resistivity/resistance method (ERM) · Evaporation front · Temperature effect

✉ Chao-Sheng Tang
tangchaosheng@nju.edu.cn

Ni An
Ann@cardiff.ac.uk

Qing Cheng
chengqing@nju.edu.cn

De-Yin Wang
wangdeyin_nju@163.com

Bin Shi
shibin@nju.edu.cn

[1] School of Earth Sciences and Engineering, Nanjing University, 163 Xianlin Avenue, Nanjing 210023, China

[2] Geoenvironmental Research Centre, Cardiff School of Engineering, Cardiff University, Newport Road, Cardiff CF24 3AA, UK

Introduction

Evaporation is of great importance in water and energy transfer between soil and atmosphere interaction. The drying process may lead to soil cracking, salinization, degradation, and other problems in arid and semi-arid areas (Shimojima et al. 1996; Tang et al. 2011b, 2018; Xue and Akae 2012; Zeng et al. 2015; Wang et al. 2016, 2018; An et al. 2017; Tollenaar et al. 2018; Li et al. 2019; Zeng et al. 2019). Therefore, the investigation of evaporation is significant to evaluate the safety of geotechnical constructions during drought periods (Saito et al. 2006; Cheng et al. 2020; Tang et al. 2019). In addition to numerical models (Penman 1948; Wilson et al. 1994; Singh and Xu 1997; Aluwihare and Watanabe 2003; An et al. 2018a), various experimental approaches have also been developed to investigate the

evaporation process, such as evaporation pan (Kondo et al. 1990; Wilson et al. 1997), soil column testing system (Wilson et al. 1994), lysimeter (Qiu et al. 1998; Newson and Fahey 2003; Teng and Yasufuku 2015), wind tunnel (Shahraeeni et al. 2012), and environmental chamber (Mohamed et al. 2000; Song et al. 2014; Teng et al. 2014). Essentially, the evaporation process can be estimated by the temporal and spatial variations of soil water content (Wilson et al. 1994; Song et al. 2014; An et al. 2018b).

Generally, the main approaches to measure soil moisture variations in laboratory and filed evaporation tests (Cahill and Parlange 1998; Aluwihare and Watanabe 2003; Tarboton 2003; Lal and Shukla 2004; Cui et al. 2010, 2013; Toll et al. 2013; Smethurst et al. 2012; Song et al. 2014) include four types: thermogravimetric, dielectric, suction-based, and geophysical methods. As a direct method, thermogravimetric measurement is to record the variations of soil sample weight to estimate the soil water content (Bittelli 2011). Dielectric approach, such as ThetaProbe and TDR, provides the water content results by exploiting the effect of liquid water dielectric permittivity on the bulk soil dielectric properties (Bittelli 2011). Suction-based sensor, such as tensiometer, is designed to estimate soil moisture by directly measuring the tension between soil particles and water molecules. As a common type of geophysical method, electrical resistivity/resistance method (ERM) measures soil resistivity/resistance by recording the changes in voltage between two electrodes caused by the transferred current (Archie 1942; Binley et al. 1996; Binley and Kemna 2005; Chambers et al. 2008; Tso et al. 2017). The main advantages and drawbacks of each method are detailed in Table 1. The distribution and variation of water content in soil samples cannot be continuously monitored by the thermogravimetric method during the test even though it is simple, economical, and accurate. More importantly, it is a highly destructive method. Time domain reflectometers (TDR), ThetaProbe, and tensiometers have been employed commonly in previous studies to monitor the variations of soil water content at specific positions (Cahill and Parlange 1998; Aluwihare and Watanabe 2003; Tarboton 2003; Lal and Shukla 2004; Cui et al. 2010; Toll et al. 2013; Smethurst et al. 2012; Song et al. 2014). However, the installation of these sensors may alter soil microstructure and the flow path of pore liquid by disturbing soil in small-scale tests (Rothe et al. 1997). Especially, the sensors' size poses a real challenge for researchers attempting to measure soil water content variations in the near-surface zone (Song et al. 2014; Teng et al. 2014). Therefore, the application of the abovementioned point-based methods of soil water content measurement exerts some limitations in small-scale laboratory evaporation test.

Compared with the point-based methods, ERM indeed has several advantages, such as non-intrusive measurement, the high spatial resolution of centimeter-level, and the opportunity to probe greater depths and to characterize the structure of the whole soil profile (Brunet et al. 2010; Samouëlian et al. 2005). As a result, it was commonly used in various aspects, including soil moisture investigation (Rhoades et al. 1976; McCarter 1984; Kalinski et al. 1993), water salinity or contaminant detection (Benson et al. 1997; Rhoades et al. 1977, 1990; Martínez-Pagán et al. 2010), buried artifacts or structures location in archeological surveys (Negri et al. 2008; Tonkov and Loke 2006), and subsurface desiccation cracks inspection (Jones et al. 2014; Gunn et al. 2015; Tang et al. 2018; An et al. 2020). Concerning the application of ERM in the estimation of soil moisture, Zhou et al. (2001) and Zhou (2007) obtained a satisfactory estimation about the 3D distribution of soil water content in a site investigation based on Archie's relationship. Besides, Alamry et al. (2017) addressed the feasibility of ERM to monitor spatial and temporal soil moisture

Table 1 A summary of four different methods to measure soil water content

Methods	Advantages	Drawbacks
Thermogravimetric method	Simple, economical, and accurate	Time-consuming and destructive; Impractical for large and massive samples, and field soil moisture distribution (Bittelli 2011)
Dielectric method (ThetaProbe, TDR)	Accurate and easy; Applicable for field and large-scale laboratory model test	Not suitable for soil sample in small size or near soil surface region; Highly sensitive to soil salt content (Wyseure et al. 1997; Bittelli 2011)
Suction-based method (tensiometer)	Economical, easy, and non-destructive	Not suitable for fine-textured soils or cold temperature (below zero); Poor adaptation in dry conditions with high soil suction (< 1.5 MPa) (Cui et al. 2005, 2013; Toll et al. 2013)
Geophysical method (ERM)	Non-intrusive; Applicable for various scales from the macroscopic to field test; Applicable for temporal monitoring of soil moisture distribution (Samouëlian et al. 2005)	Calibration is required within different soil units under controlled conditions (Samouëlian et al. 2005)

in a semi-arid area for non-accessible soils and weathered substrates. Many other similar types of research have been carried out to map soil moisture distribution based on ERM in field surveys considering rainfall (Brunet et al. 2010; Beff et al. 2013; Gunn et al. 2015; Faměra et al. 2018). Various empirical relationships were developed in the abovementioned studies for the determination of soil moisture from the geoelectrical measurement. In general, soil water content presents an inverse relationship with the variation of electrical resistivity (Samouëlian et al. 2005). The abovementioned studies mainly present the satisfactory performance of ERM in various field surveys. However, to the authors' best knowledge, comprehensive investigation addressing the application of ERM in small-scale laboratory evaporation tests to estimate the soil moisture dynamics is still absent.

The objective of this paper is to develop ERM with a high spatial resolution and study the application of ERM to characterize the soil water content dynamics from a quantitative point of view in small-scale laboratory evaporation tests. Four different evaporation tests were carried out with recording the temporal and spatial variations of soil electrical resistance. The effect of soil temperature on the measured soil electrical resistance was evaluated. The relationship between soil gravimetric water content and corrected electrical resistance considering the effect of soil temperature was developed for the studied sandy soil and then validated by the experimental results. The drying process with the movement of the evaporation front was also discussed in depth.

Materials and methodology

Materials and specimen preparation

The soil used in this investigation is commercial silica sand in a particle size range of 0.2~0.55 mm. The specific gravity of commercial silica sand is 2.65.

The size of the prepared soil sample is 84 mm and 290 mm in diameter and height, respectively, as shown in Fig. 1a. A plexiglass column with a thickness of 5 mm was designed to contain the soil sample. In order to ensure soil homogeneity, the funnel method (Miura and Toki 1982; Vaid and Negussey 1998; Hakhamaneshi et al. 2016) was performed to prepare the sandy soil samples with an average dry density of 1.48 g/cm^3 and porosity of 0.44.

Eight groups of initially saturated soil samples (T1 and T2 for test 1, T2 for test 2, S1, S2, S3, S4, and S5 for test 3, and S6 for test 4) were prepared to study the variations of soil water content and electrical resistance during drying. An injection tube with a diameter of 8 mm was connected to the soil sample for the purpose of continuous water supply (Fig. 1a). The saturation process of soil samples, T1 and T2, was conducted by supplying deaired water constantly from a water container through the injection tube (Fig. 1b). It took around 5 h to saturate the soil sample. During the saturation process, the water level in the container was elevated gradually and kept higher than the top surface of the soil columns. Specifically, the water level was kept around 5 min after being elevated every 5 mm to ensure the effective drainage of air bubbles in soil. The elevation of water level stopped until it was 5 mm higher than the soil top surface. The soil sample was assessed as fully saturated after observing the water exfiltration on the soil surface, and this stage was kept for around 1 h. The other six groups of soil samples (S1, S2, S3, S4, S5, and S6) followed the same saturation procedure.

Experimental setup

Due to the high association between soil physical properties and electrical resistance/resistivity distribution in soil samples, ERM can be applied as an appealing approach to assess the spatial and temporal variations of soil water content (Archie 1942; Goyal et al. 1996; Alamry et al. 2017). Soil electrical resistivity can be monitored using a variety of electrode configurations including one-, two-, and four-electrode methods (Samson et al. 2018). Generally, the Wenner array in four-electrode method is most commonly used in the field (Dahlin 2001; Wang et al. 2012). The value of soil electrical resistivity is usually estimated based on the injected current, the measured electrical potential, and the value of the geometrical coefficient which mainly depends on the arrangement of electrodes and test equipment (Scollar et al. 1990; Kearey et al. 2002; Tang et al. 2018). It can be used to measure the distribution of soil resistivity at various distances and depths by rearranging the electrode setup (Reichling et al. 2015). However, the application of this method in small-scale tests is limited due to the arrangement of the four electrodes.

In terms of electrical resistivity measurement of small-scale laboratory soil samples, the effect of geometric boundaries on the experimental result is difficult to be estimated (Zhou 2007). Hence, for simplicity, soil resistance was measured in this study to avoid the assessment of the geometrical coefficient in the estimation of soil electrical resistivity. Besides, the arrangement of four electrodes in the soil is over complicated due to the small size of the studied soil sample and the specialized cylindrical container. Therefore, a two-electrode method was applied in this study (Reichling et al. 2015; Samson et al. 2018).

In order to get a relatively high spatial resolution of the measured resistance, eight couples of electrode holes were reserved at eight depths in a vertical distance of 30 mm, on two parallel lines (L1 and L2) of the plexiglass column (Fig. 1). Afterwards, eight couples of mini electrodes were installed at these positions with different depths: #1–1′ (30 mm), #2–2′ (60 mm), #3–3′ (90 mm), #4–4′ (120 mm), #5–5′ (150 mm),

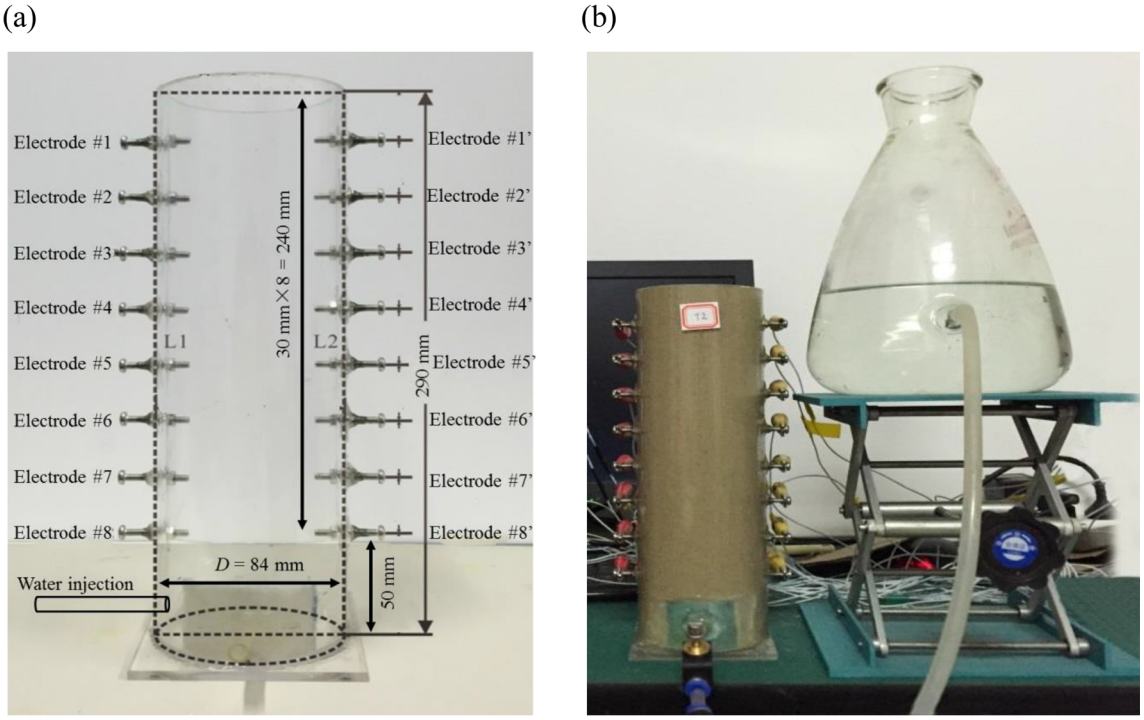

Fig. 1 The details of (**a**) column module for evaporation test and (**b**) soil sample saturation process

#6–6′ (180 mm), #7–7′ (210 mm), and #8–8′ (240 mm). The adopted electrodes were fabricated using stainless steel bolts with a length of 33 mm and a diameter of 3.5 mm, so that they were installed manually with convenience. The effect of electrode size on the measured results was minimized by using the electrodes with reasonably small diameters. The bottom of the soil column was fixed by an impermeable plexiglass sheet of 110 × 110 mm.

Figure 2a presents the developed ERM setup. It includes an ambient temperature and relative humidity monitoring system (ATRM), an electrical resistance acquisition system (ERA), and the prepared soil sample. The variations of ambient temperature and relative humidity during the test were recorded by the TES-1370 type of ATRM. It was mounted 30 cm above soil samples to reduce the possible influence of drying on the measured relative humidity values. ERA consists of TH2819A precision LCR meter (LCR), a programmable logic controller (PLC), logic control part, and electrodes on the soil sample. LCR was used to measure the soil electrical resistance between every two electrodes based on the bridge method (Aoki and Yokoi 1997; Maeda 1974). In this test, two linked PLC were employed to control the electrode combination. Eight electrodes at the left side and eight electrodes at the right side of the soil column were connected to PLC as shown in Fig. 2a. The measuring lines M and N of two PLC were connected to ports A and B of LCR, respectively. The logical control lines of both LCR and PLC were then connected to the recording computer system. Eight groups of resistance data (#1–1′, #2–2′, #3–3′, #4–4′, #5–5′, #6–6′, #7–7′, and #8–8′) were obtained by running LCR. All the sensors used in this measuring system were calibrated before starting the test. Because the sample was small enough to stabilize the heat transfer rapidly, the soil temperature was assumed to be the same as the measured ambient temperature.

Testing procedure

Test 1—saturated versus unsaturated soil samples

Test 1 was performed to study the variations of electrical resistance of soil samples T1 and T2 during their stabilization processes. After the initial saturation process, these two soil samples were exposed to air to dry freely. During the drying process, the water container was kept connected to soil sample T2 after its initial saturation process, but it was removed in the case of soil sample T1. The variations of soil electrical resistance at different depths were recorded every 30 min by ERA.

The drying test was conducted for around 260 h in an underground laboratory, which is favorable to provide a relatively stable atmospheric condition. The measured ambient temperature is around 20 ± 0.5 °C and the average relative humidity is 97.81% under the control of the air conditioner during the studied period.

Test 2—temperature effect

Hayley et al. (2007) have pointed out the importance to consider the effect of soil temperature on soil electrical resistivity.

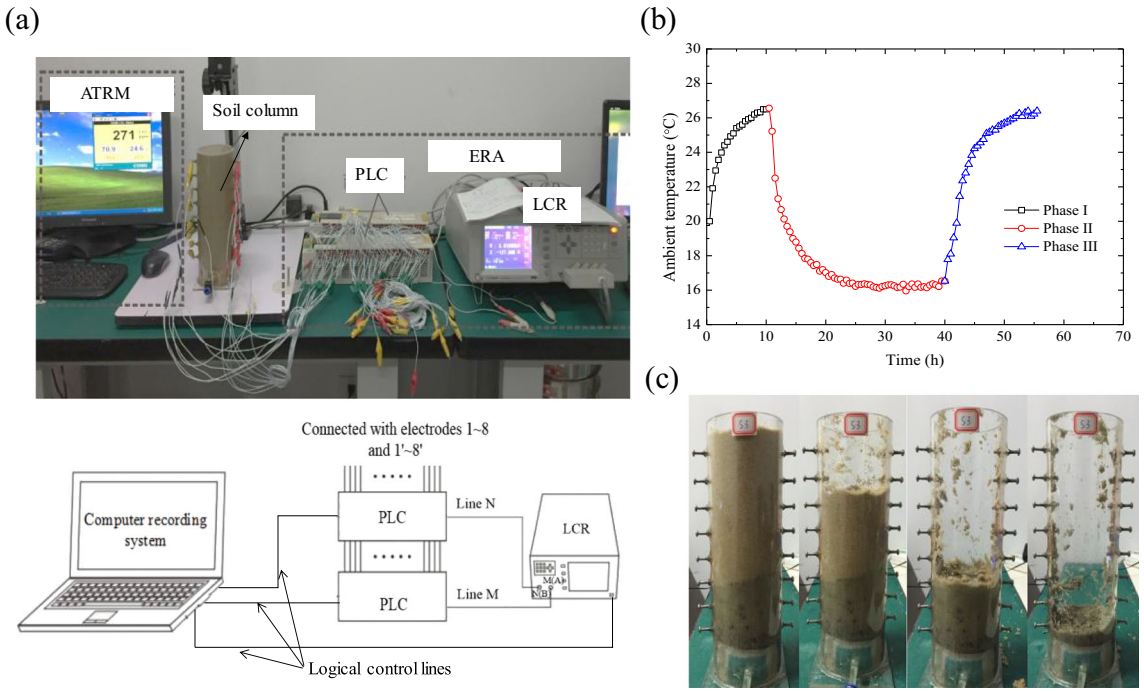

Fig. 2 **(a)** Experimental setup of soil column evaporation test and the details of ERM system, **(b)** the variations of ambient temperature in test 2, and **(c)** the process of removing soil layer at different depths for gravimetric water content measurement in test 3

Soil sample T2 was further applied to evaluate the effect of soil temperature on the variations of the measured electrical resistance in this study. Test 2 was implemented with a three-phase (phase I heating - phase II cooling - phase III heating) process of ambient temperature control (Fig. 2b). The initial ambient temperature was 20.0 °C. In the first phase, the air conditioner's temperature was elevated to 26.5 °C, then the average ambient temperature grew up gradually to 26.5 °C. After 10 h, cooling change was operated in phase II by setting the air conditioner at 15 °C. As a result, the ambient temperature decreased to 15 °C gradually. Phase III started at $t = 40$ h by resetting the air conditioner's temperature at 26.5 °C, which was maintained for 15 h to allow the ambient temperature to reach the same value. During the studied period, the ambient temperature was recorded every half an hour by the monitoring system, and the data of measured soil electrical resistances was also collected every 30 min.

Test 3—calibration of the relationship between soil electrical resistance and water content

The objective of test 3 is to calibrate the relationship between soil electrical resistance and gravimetric water content through the measurements of five parallel soil samples (S1, S2, S3, S4, and S5). After the initial saturation, their connections with the water container were removed. The five soil samples were sealed and kept for 3~4 days in order to obtain the initial stabilization. Afterwards, they were subjected to drying for 44.5 h (S1), 122 h (S2), 429 h (S3), 577.5 h (S4), and 811.5 h (S5), respectively, in the same environmental condition. The measured results of soil electrical resistances at different depths of each sample were collected every 30 min.

At the end of each sample test, soil layers at different depths were taken out following the steps (Fig. 2c): the topsoil layer of 15 mm was removed firstly; soil layer located at both 15 mm above and 15 mm below the positions of electrode couple #1–1′ was taken out; soil layers around electrode couples #2–2′, #3–3′, #4–4′, #5–5′, #6–6′, #7–7′, and #8–8′ were also removed following the same procedure as electrode couple #1–1′. They were used for the gravimetric water content measurements at eight different depths of each soil sample through the oven drying method. In other words, the values of soil gravimetric water content and electrical resistances at 40 points at the end of Test 3 were collected. Based on these data, a calibration relationship between soil gravimetric water content and electrical resistance can be developed.

Figure 3 presents that the measured average ambient temperature is around 18.09 °C and the average relative humidity is around 92.22% during the studied period of test 3.

Test 4—validation of the calibration relationship

Soil sample S6 was applied in test 4 to verify the calibration relationship developed based on the results of test 3, and to study the evolution of the average water content as well as the evaporation rate. After its initial saturation, the connection with water container was removed, and soil sample S6 was subjected to continuous drying in the laboratory. It was performed

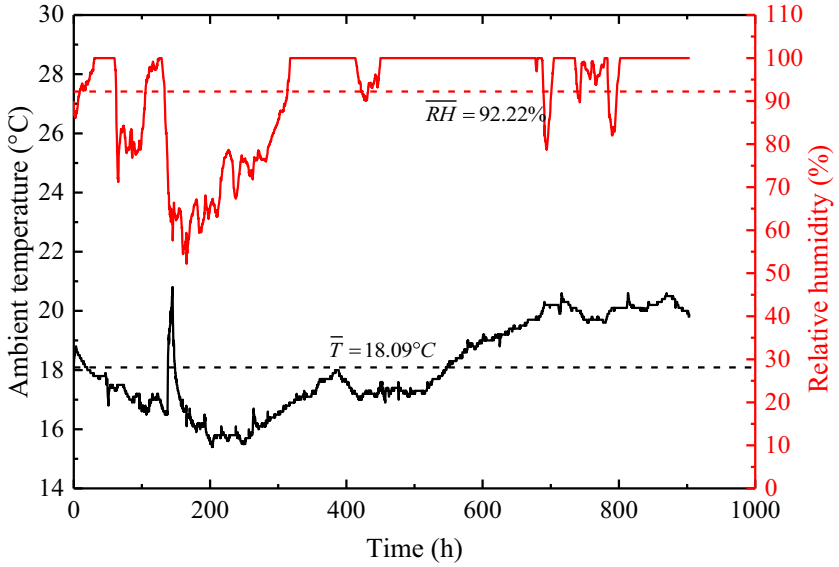

Fig. 3 The variations of ambient temperature (average value of 18.09 °C) and relative humidity (average value of 92.22%) in tests 3 and 4

synchronously with the other five soil samples in test 3 in the same environmental condition. The soil electrical resistances at different depths of soil sample S6 were also recorded every 30 min. At the end of test 4, soil layers at different depths of soil sample S6 were taken out for water content measurement following the same procedure as soil sample S1. Moreover, the mass of soil sample S6 was recorded at different times, which was applied to investigate the evolutions of the soil average water content and the actual evaporation rate. The soil average water content was calculated based on the difference between soil total mass and its dry mass. The water loss estimated by the change of soil sample mass was recorded to calculate the evaporation rate. In addition, the main information of four different tests is detailed in Table 2 for highlighting their ambient conditions and research objectives.

Results

Test 1—saturated versus unsaturated soil samples

The variations of measured electrical resistances of soil samples T1 and T2 during their stabilization processes are presented in Fig. 4a and b, respectively. Obvious differences can be observed between the results of soil samples T1 and T2. In the case of soil sample T1 (Fig. 4a), soil electrical resistances recorded by electrode couples #1–1′ and #2–2′ are relatively stable during the first 38 and 58 h, respectively. Afterwards, the measured result of electrode couple #1–1′ goes up quickly and keeps a high increasing rate until the end of test 1 with small fluctuations around $t = 175$ h. Soil electrical resistance of electrode couple #2–2′ increases continuously after the stable stage. However, the measured result of electrode couple #3–3′ starts to increase from $t = 152$ h until the end of test 1. The significant increases in the soil electrical resistances of these three depths are mainly attributed to the decreases in soil water content of the near-surface area. The delaying response of soil electrical resistance along a depth gradient is mainly related to the drying-induced variations of water content. Measurements of electrode couples #4–4′, #5–5′, #6–6′, #7–7′, and #8–8′ are relatively constant values during the whole studied period. It indicates that the water contents in the deeper zone (depth > 120 mm) are not influenced by the surface evaporation, and the soil is close to a saturated state during the drying process. The stable value of measured

Table 2 A summary of the experimental conditions and objectives of four evaporation tests

Test no.	Soil samples	Ambient temperature (°C)	Average relative humidity (%)	Test aim
1	T1 and T2	20 ± 0.5	97.81	To study the variations of electrical resistance of soil samples T1 and T2 during their stabilization processes
2	T2	26.5 (phase I) 15.0 (phase II) 26.5 (phase III)	Not measured	To evaluate the effect of ambient temperature on the variations of soil electrical resistance
3	S1, S2, S3, S4, and S5	18.09 (average value)	92.22	To calibrate the relationship between soil electrical resistance and gravimetric water content
4	S6	18.09 (average value)	92.22	To verify the calibration relationship developed based on the results of test 3, and to study the evolution of the average water content as well as the actual evaporation rate

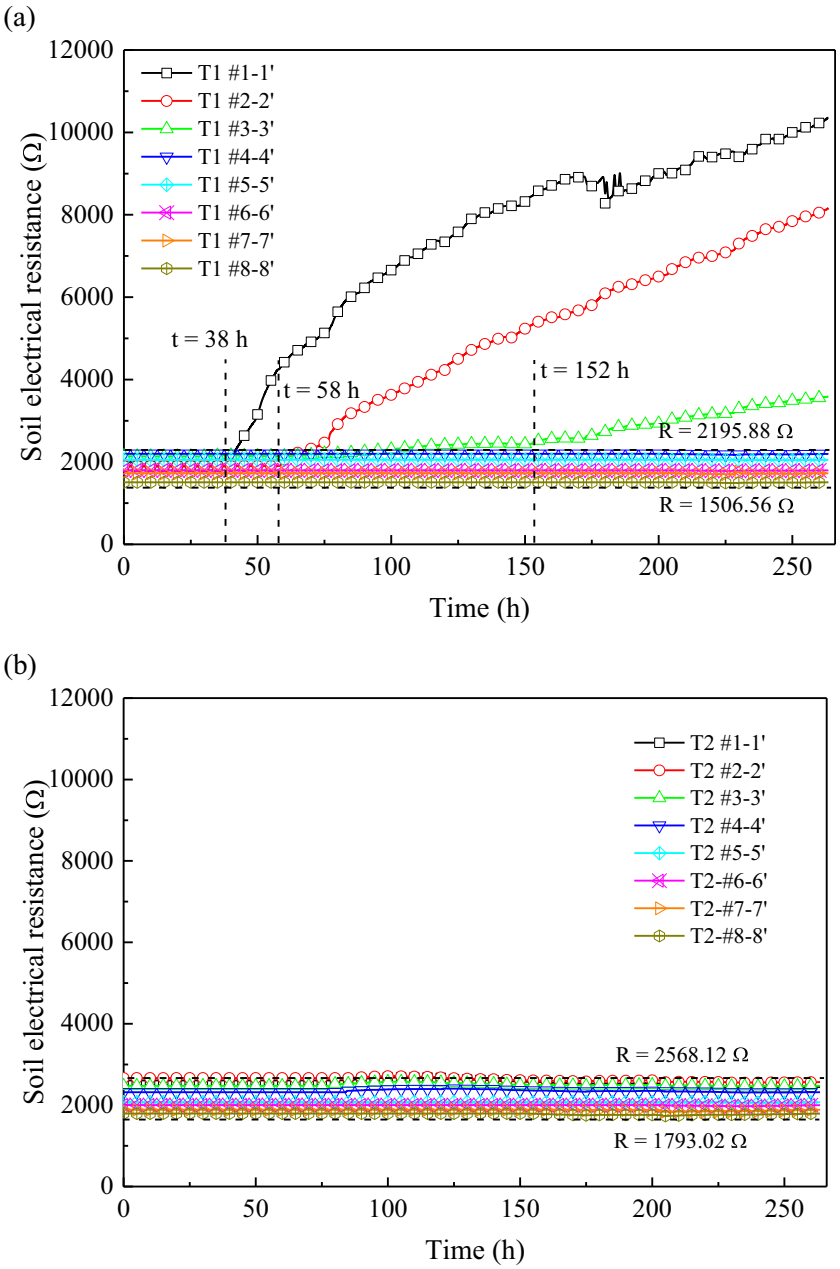

Fig. 4 The variations of the measured soil electrical resistances versus time in test 1: soil samples (**a**) T1 and (**b**) T2

soil electrical resistance decreases from 2195.88 (electrode couple #4–4′ at a depth of 120 mm) to 1506.56 Ω (electrode couple #8–8′ at a depth of 240 mm) as the depth increases. Theoretically, the variations of soil electrical resistance may also be affected by the contact condition between soil particles and electrodes during the drying process. The compaction condition of soil particles in the deeper zone contributes to higher soil density. More compact soil has a lager soil electrical conductivity as well as lower soil electrical resistance when soil is in a saturated state. Hence, it explains that soil electrical resistance presents a decreasing tendency versus depth in the deeper zone (depth > 120 mm).

In the case of soil sample T2 (Fig. 4b), the measured soil electrical resistances at different depths generally show stable values during the whole studied period. It is attributed to the fact that soil sample T2 keeps saturated by the continuous water supply. The relationship between the values of soil electrical resistances and the corresponding depths of soil sample T2 is similar to that of the deeper zone in soil sample T1. Soil electrical resistance reduces from 2568.12 Ω at a depth of 30 mm (electrode couple #1–1′) to 1793.02 Ω at a depth of 240 mm (electrode couple #8–8′) due to the effect of soil compaction condition.

Test 2—temperature effect

As shown in Fig. 5a, the measured soil electrical resistances at the different depths follow the same variation tendency: they decrease in the first 10 h (phase I) then go up until $t = 40$ h (phase II) and show a decreasing trend until the end of the test (phase III). The variation pattern of the measured electrical resistances presents a high correlation with the ambient temperature variations (Fig. 2b): soil electrical resistance reduces as the ambient temperature goes up, and vice versa. Figure 5b presents the hysteresis loop variations of soil electrical resistance at different depths along with the three-phase variation of ambient temperature, confirming the decreasing variation tendency of soil electrical resistance as the ambient temperature increases. Moreover, it is observed that soil electrical resistance in the 3rd phase is slightly higher than that at the same temperature in the 1st phase, which may be attributed to the thermal-induced slight change of soil microstructure in the 1st and 3rd phases caused by the cyclic temperature change. However, further investigation is still required to clarify this point.

Soil temperature is assumed to be the same as the measured ambient temperature, as explained in the "Experimental set-up" section. As the main component of sandy soil, quartz has very low electrical conductivity. Consequently, the electrical resistance of the studied soil sample is mainly influenced by

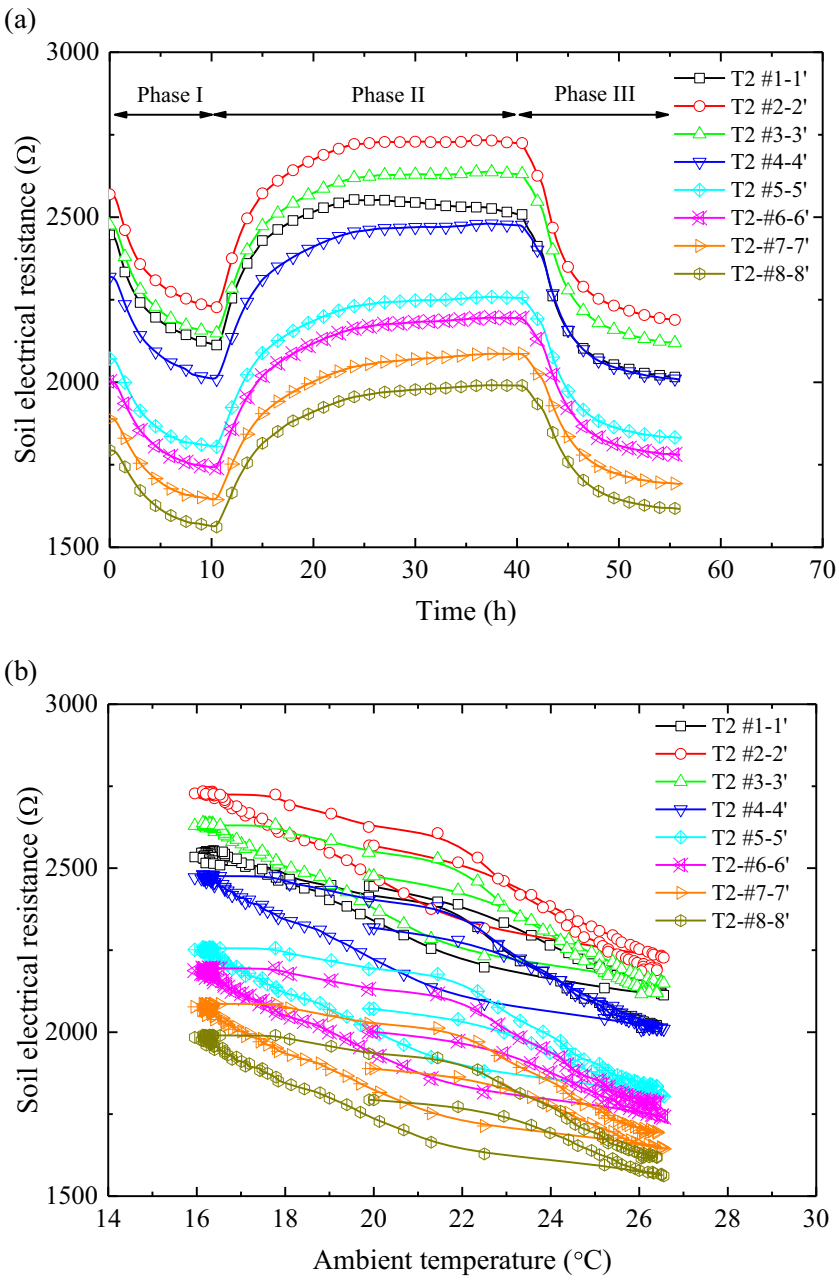

Fig. 5 In test 2, the variations of measured soil electrical resistances at different depths versus (**a**) time and (**b**) ambient temperature

the amount and continuity of pore water and water electrical conductivity. The amount and continuity of pore water in soil sample T2 are constant due to its saturated state during test 2. Thereby, the variations of soil electrical resistance of sample T2 is significantly affected by the water electrical conductivity. As soil temperature goes up, pore water viscosity decreases gradually, leading to an increase of ions' mobility in soil and water electrical conductivity (Archie 1942; Pitzer 1982; Zha et al. 2007). It explains the decreases in soil electrical resistance as soil temperature increases. In order to consider the temperature effect, Keller and Frischknecht (1966) proposed to correct the measured soil electrical resistivity to its values at a standard temperature of 25 °C:

$$\rho_{25} = \rho_T(1 + \alpha(T-25)) \quad (1)$$

where ρ_T and ρ_{25} represent the soil electrical resistivities at measured temperature T and standard temperature of 25 °C, respectively; α is an empirical coefficient, equals to 0.025 °C^{-1} (Keller and Frischknecht 1966; Brunet et al. 2010; Ackerson et al. 2014). It means that a variation of 1 °C in the temperature leads to a deviation of 2.5% in the value of soil electrical resistivity. Similarly, in this study, the influence of soil temperature on the measured value of soil electrical resistance can be considered by the following:

$$R_{25} = R_T(1 + \alpha(T-25)) \quad (2)$$

where R_T and R_{25} represent the soil electrical resistances at temperatures T and 25 °C, respectively. Based on the variations of measured soil electrical resistance in the 1st phase with the temperature varying from 19.9 to 26.5 °C, the empirical coefficient α was experimentally checked in this test. The fitted values of α for the results at eight depths are detailed in Table 3, providing its average value as 0.022 °C^{-1}. In the following work, the measured electrical resistances have always been corrected to its value at a standard temperature of 25 °C.

Test 3—calibration of the relationship between soil electrical resistance and water content

Based on the water content profiles of the five soil samples (measured by the oven drying method) in test 3, it can be observed that soil water content in the near-surface zone decreases quickly due to the surface drying, whilst the bottom soil keeps a saturated state during the whole studied period (Fig. 6a). Specifically, in the soil water content profile of sample S5, the values of water content at the three points near the soil surface are very close. It is therefore inferred that soil at these points is close to the dry state at $t = 811.5$ h.

It is noticed that the ambient temperature is not constant during the studied period of test 3 (Fig. 3). Therefore, the measured soil electrical resistance needs to be corrected based on Eq. (2) with consideration of the soil temperature effect. Among the five parallel soil samples, soil sample S5 is taken as the representative to show the variations of corrected electrical resistance at the depths of eight couples of electrodes #1–1′, #2–2′, #3–3′, #4–4′, #5–5′, #6–6′, #7–7′, and #8–8′ (Fig. 6b). Soil electrical resistances at the depth of electrode couples #1–1′ and #2–2′ both increase gradually during the whole studied period. However, the values at the depth of electrode couple #2–2′ become larger than that of electrode couple #1–1′ after around 200 h. It may be due to the presence of soil heterogeneity in the near-surface area and the influence of the contact condition between the soil and the installed electrodes during the drying process. After different periods, the measured results of electrode couples #3–3′, #4–4′, and #5–5′ start to increase at different rates and keep the increasing trend until the end of test 3. It is observed that soil electrical resistance at the deeper position keep the initial values for a longer period, and then increases at a lower rate. However, the results of electrode couples #6–6′, #7–7′, and #8–8′ keep relatively constant values during the whole studied period.

The relationship between the variations of soil water content and corrected electrical resistances has been developed in power (Archie 1942; Frohlich and Parke 1989), linear (Goyal et al. 1996; Gupta and Hans 1972), polynomial (Rhoades et al. 1976), and exponential (Zhu et al. 2007) empirical models. Calamita et al. (2012) stated that the three types of non-linear models (power, polynomial, and exponential) are the most common methods applied in literature and presented the good agreement between the moisture–resistance relationships derived by different methods. It is agreed that the differences between them are not significant, especially in the application with a limited range of variation of the variables (Zhu et al. 2007; Calamita et al. 2012). Indeed, the soil moisture–resistance relationship is influenced by many factors in terms of water and soil characteristics, such as porosity, texture, salinity, and temperature.

Table 3 The fitted values of empirical coefficient α and the corresponding adjusted R-squared ($Adj\ R$) for the measured soil electrical resistance-temperature relationship at the depths of eight electrode couples

Electrode couples	#1–1′	#2–2′	#3–3′	#4–4′	#5–5′	#6–6′	#7–7′	#8–8′
α	0.02205	0.02207	0.025	0.02203	0.02198	0.02202	0.02191	0.02173
$Adj\ R$	0.97625	0.97002	0.94059	0.95393	0.95129	0.947	0.93941	0.92977

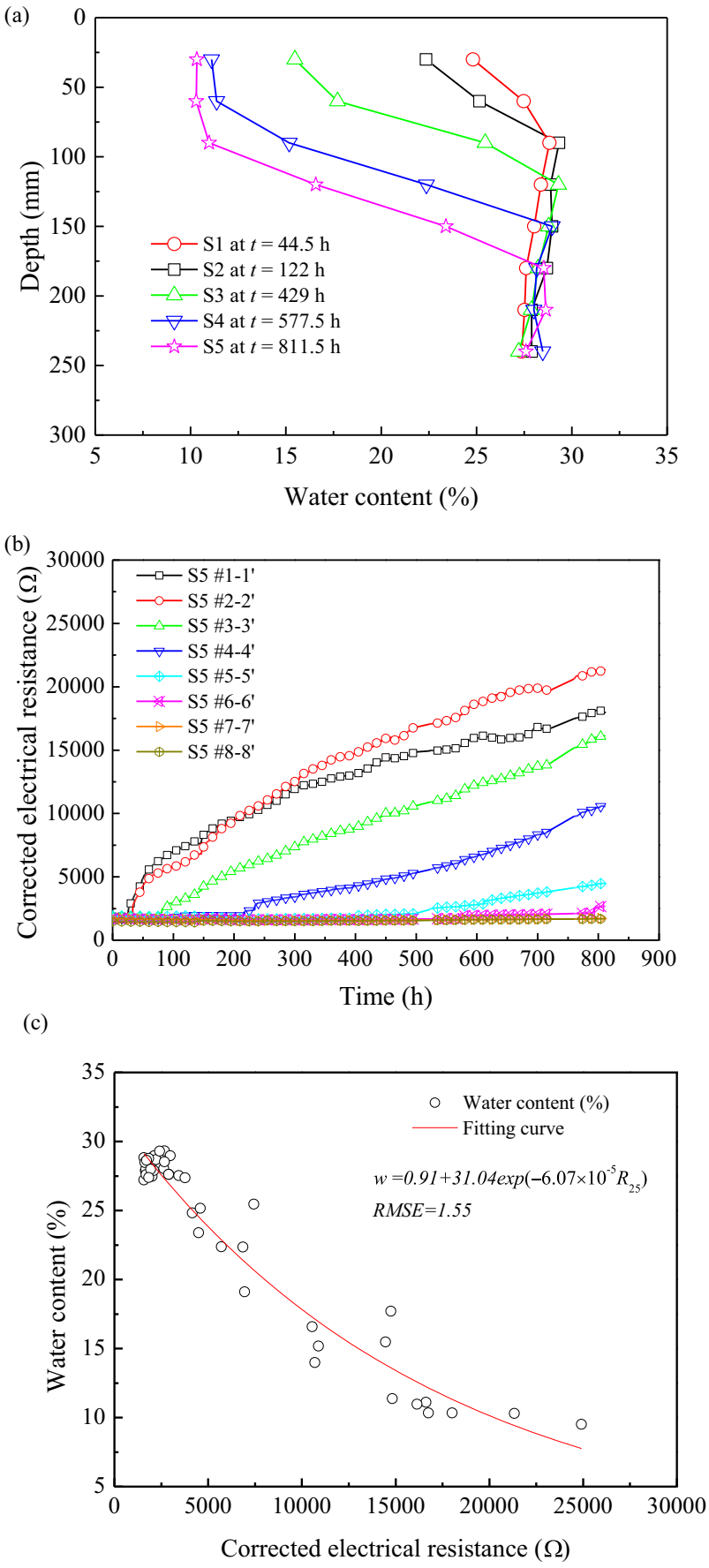

Fig. 6 In test 3, (**a**) the variations of the measured soil water content at different moments of soil sample S1, S2, S3, S4, and S5; (**b**) the variations of the corrected electrical resistances versus time for soil sample S5; and (**c**) the fitting curve of the relationship between the corrected electrical resistance and water content at the measured points

In this study, the variation of the measured soil water contents versus corrected electrical resistances presents an exponential tendency, as shown in Fig. 6c. Hence, the exponential model is adopted to fit the soil moisture–resistance relationship considering the temperature effect. It is expressed by the following:

$$w = 0.91 + 31.04e^{-6.07\times10^{-5}R_{25}} \quad (3)$$

where w is the soil gravimetric water content. Soil water content decreases gradually as electrical resistance increases. Based on the corrected electrical resistances, the predicted soil water contents at the studied points are calculated, presenting a standard deviation of the prediction errors (RMSE) as 1.55 compared with the measured values (Fig. 6c).

Test 4—validation of the calibration relationship

Test 4 was performed in the same atmospheric condition as the five soil samples in test 3 (Fig. 3). As shown in Fig. 7a, the measured results of both electrode couples #1–1′ and #2–2′ present a continuous increase tendency during the whole studied period. However, the measured results of electrode couples #3–3′, #4–4′, #5–5′, and #6–6′ start to go up after different periods. The increasing rate of soil electrical resistance decreases as the measured point goes deeper. In terms of the bottom couples of electrodes #7–7′ and #8–8′, soil electrical resistances keep relatively stable values during the whole drying process.

Figure 7b presents that the actual evaporation rate fluctuates from the beginning and reaches the highest value of 1.9 mm/day at t = 160 h. Afterwards, the actual evaporation rate shows a

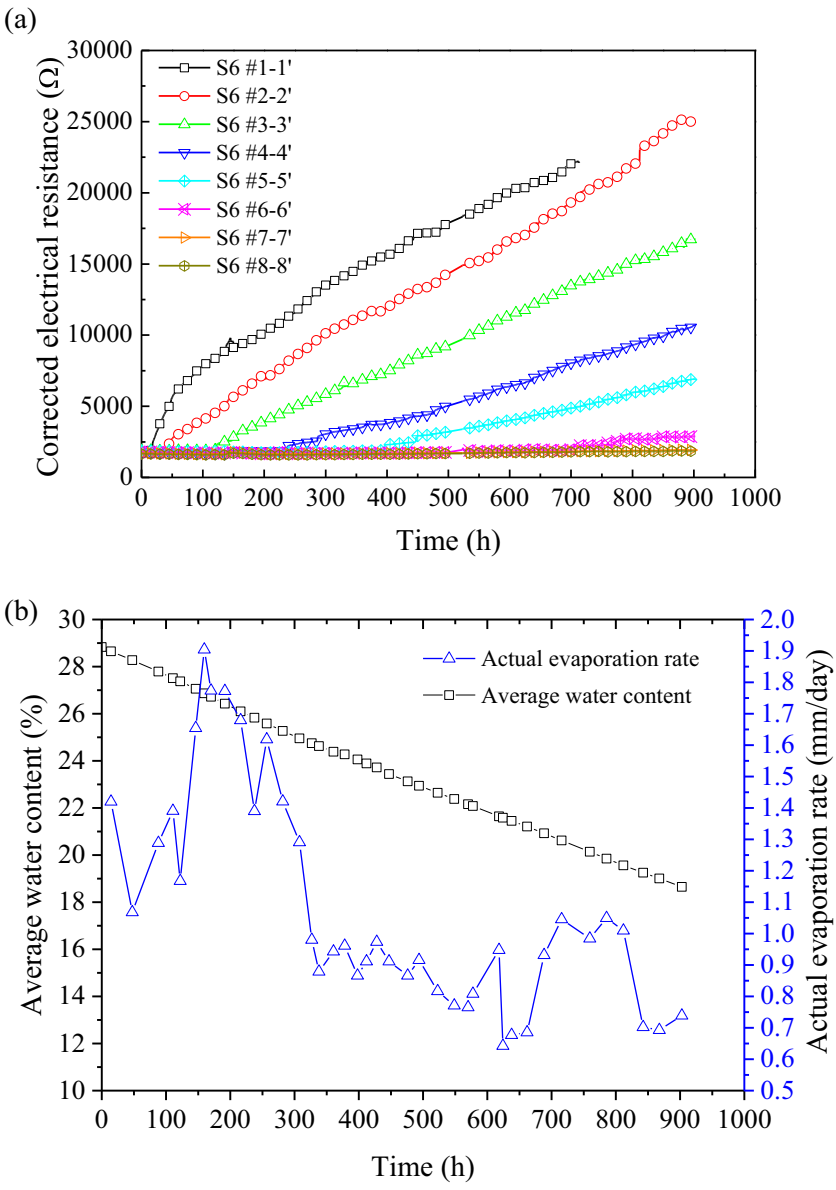

Fig. 7 For soil sample S6 in test 4, (**a**) the variations of the corrected electrical resistance at different depths during the studied period and (**b**) the variations of the soil average water content and the actual evaporation rate versus time

general decreasing tendency with a slight rebound at $t = 256$ h. From 338 to 550 h, the actual evaporation rate presents slight fluctuations, varying in the range of 0.85~1 mm/day. It is followed by larger fluctuations until the end of the studied period. Generally, with a stable atmospheric condition, water evaporation from soil surface occurs normally in three stages: constant rate stage, falling rate stage, and residual stage (Wilson et al. 1994; Aluwihare and Watanabe 2003; An et al. 2018b). However, the three stages are not identified in the evaporation evolution, due to the predominant effect of varying ambient temperature and relative humidity in test 4. The soil average water content shows a steady decreasing trend as the evaporation continues (Fig. 7b).

Based on the experimental results of soil sample S6 during the drying process, the calibration relationship between soil water content and corrected electrical resistance considering soil temperature effect is validated by the following two steps:

In the first step, at the end of test 4 ($t = 902.5$ h), due to the absence of measured result by electrode couple #1–1′, the corrected soil electrical resistance at depths of 60 mm (electrode couple #2–2′), 90 mm (electrode couple #3–3′), 120 mm (electrode couple #4–4′), 150 mm (electrode couple #5–5′),

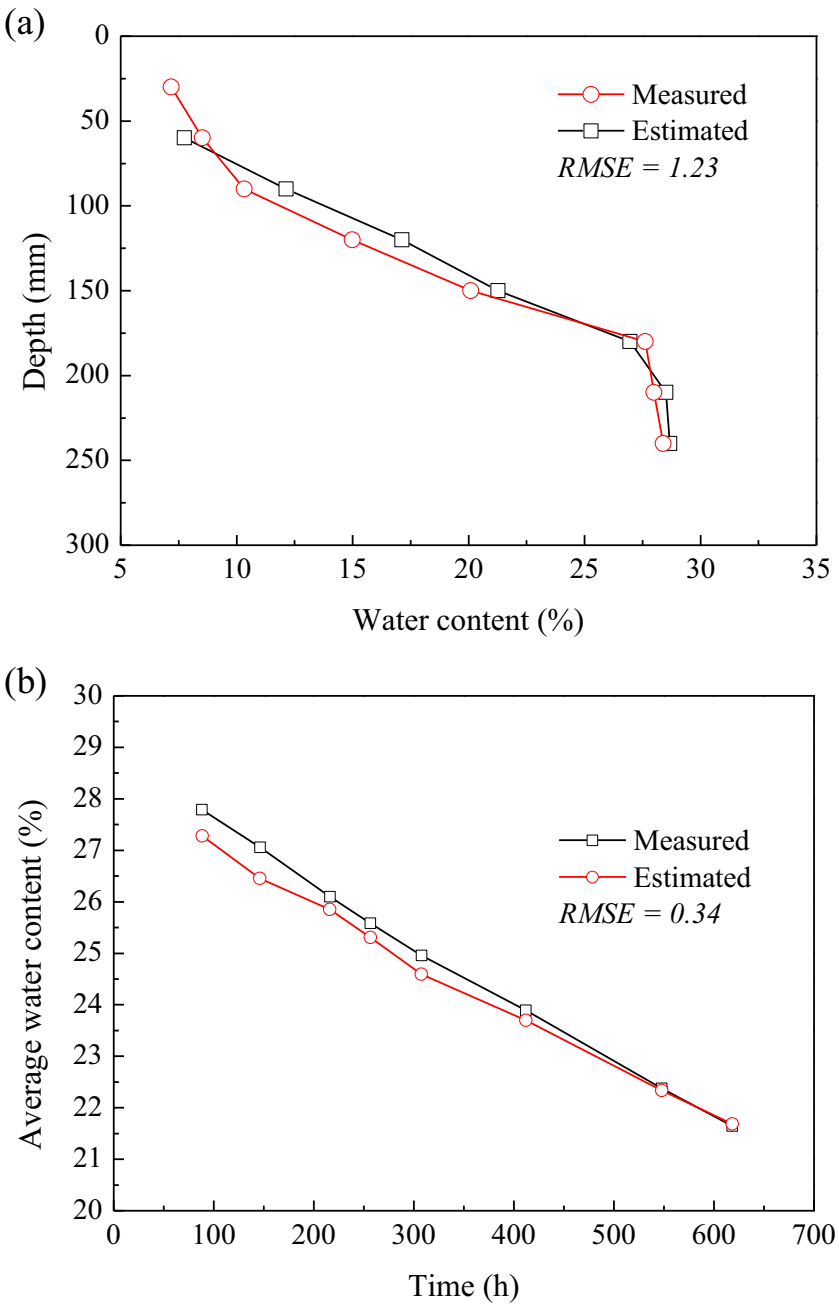

Fig. 8 For soil sample S6 in test 4, (**a**) the comparison between the estimated and measured soil water content at different depths ($t = 902.5$ h), and (**b**) the comparison between the estimated and measured average soil water content at different moments

180 mm (electrode couple #6–6′), 210 mm (electrode couple #7–7′), and 240 mm (electrode couple #8–8′) is used to estimate the soil water contents. The comparison between the estimated and measured soil water content versus depth is then performed as shown in Fig. 8a. A good agreement is obtained between the measured and estimated water content (RMSE = 1.23), validating the correctness of the developed soil resistance-moisture relationship.

With the available information of measured average soil water content of soil sample S6 (Fig. 7b), the second step of verification work is conducted through comparing the measured results with the estimated average water content at different moments. In this study, the measured results at t = 88.25 h, t = 146.25 h, t = 216.17 h, t = 256.7 h, t = 307.8 h, t = 412 h, t = 548.0 h, and t = 618.3 h are employed as representatives to show the variation of the average water content during the whole studied period. The corrected soil electrical resistances at these moments are used to calculate the water content distribution in the soil sample, allowing the further estimation of the average water content. Figure 8b presents that the calculated results of average water content at these moments fit very well with the measured results (RMSE = 0.34), further validating the calibration relationship. Therefore, it indicates that the temporal and spatial variations of soil water content at different depths of the studied soil sample during the drying process can be estimated conveniently and precisely by the developed ERM.

Discussions

Based on the validated relationship between soil electrical resistance and water content (Eq. (3)), water content distributions of soil sample S6 at t = 0 h, 100 h, 200 h, 300 h, 400 h, 600 h, 700 h, 800 h, and 902.5 h are estimated as shown in Figs. 9. It is identified that soil water content at the surface zone decreases more quickly than that in the deeper zone as drying continues. The surface soil transfers gradually from saturated to unsaturated state because of the continuous drying. In contrast, the bottom soil keeps saturated due to the high resistance of the upward water movement. In addition, it is of great importance to identify the position of evaporation front during the drying process, which determines the thickness of the dry layer and influences the soil engineering properties (Shokri et al. 2008; Aluwihare and Watanabe 2003; Tang et al. 2011a). Depending on the contour of soil water content as shown in Fig. 10, it is feasible to identify the movement of the evaporation front during the drying process. Evaporation front is limited above depth of around 90 mm at t = 100 h, 110 mm at t = 200 h, 140 mm at t = 300 h, and 150 mm at t = 400 h, respectively. After 600 h, the evaporation front moves towards a deeper zone slowly. It infers that the evaporation front moves at a slower rate as it goes deeper, which may be related to the high vapor resistance in the dry layer. Further investigation is still required to clarify this point.

In the laboratory studies in terms of soil dynamics under the effect of evaporation in the literature (Wilson et al. 1994; Yanful and Choo 1997; Song et al. 2014), the traditional point-based methods (weight measurements, TDR, ThetaProbe, etc.) need to be set up within specific/proper distances in soil samples to ensure the correct measurement of soil water content. As a result, the soil moisture in the near-surface zone is difficult to be measured even though it was speculated that the evaporation from bare soil occurs mainly within a depth of 55 mm (Song et al. 2014). On the other hand, the evaporation front was visually determined by observing the color change

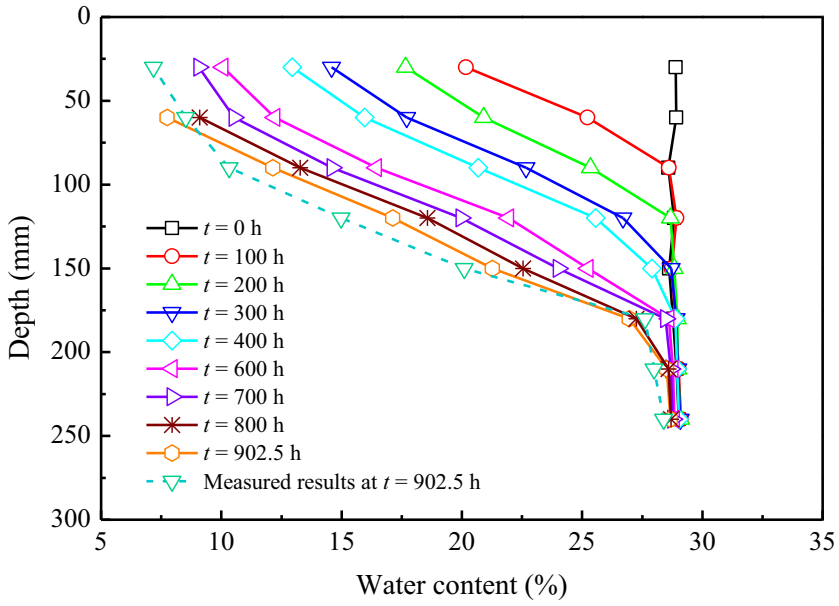

Fig. 9 The estimated soil water content profiles of soil sample S6 at different times: t = 0 h, 100 h, 200 h, 300 h, 400 h, 600 h, 700 h, 800 h, and 902.5 h during the evaporation process and the measured water content of soil sample S6 at t = 902.5 h

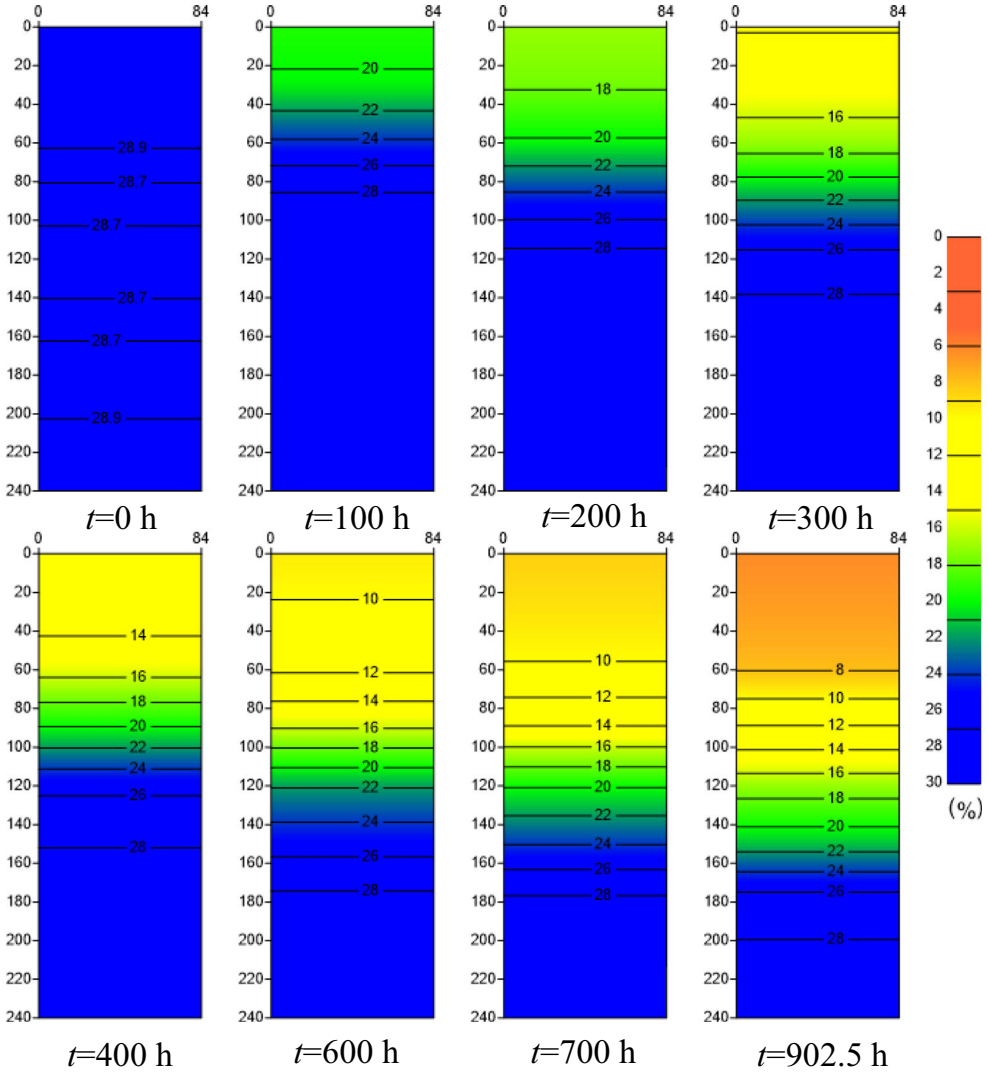

Fig. 10 The estimated soil water content distribution during the evaporation process of soil sample S6

in the top layer of soil compared with the underlying soil layer, for a fair estimation of the depth of the dry layer (van de Griend and Owe 1994; Yamanaka et al. 1997). Compared with the abovementioned studies, the results herein demonstrate the superiority of ERM in small-scale laboratory tests, especially in the quantitative analysis of temporal and spatial soil moisture variations, the soil moisture distribution in the near-surface zone, and the evaporation process with the identification of evaporation front. Theoretically, the spatial resolution of measurement based on the developed ERM can be further improved by reducing the electrode size and distance appropriately. Electrical resistivity measurements along a vertical plane in a 2D/3D laboratory model test based on four-electrode methods are also feasible. These works will be conducted in the next stage.

Furthermore, this study also presents the potential application of ERM in the field investigation of the drying process in arid or semi-arid regions where drought happens frequently and the similar dynamic of soil water content driven by evapotranspiration, irrigation, etc. Considering soil electrical characteristics is conditioned by many factors (mineral composition, grain size distribution, density, degree of saturation, etc.), detailed calibration work before any application of ERM is indispensable. More research on quantitative comparisons between different approaches of soil water content measurement and the study in cases of different soil types will be supportive of the wide applications of ERM.

Conclusions

Four different tests were conducted to investigate the application of the developed ERM in the estimation of soil water content dynamics driven by evaporation. The effect of temperature on the measured electrical resistance was evaluated by experimentally checking the empirical coefficient for the studied soil. The relationship between the corrected soil electrical resistance considering temperature effect and water

content was established for the studied soil sample. It indicates that soil electrical resistance increases exponentially as the water content decreases. The calibration relationship was validated successfully by the experimental results, suggesting that the spatial and temporal variations of soil water content during drying can be well characterized by ERM. The variations of soil electrical resistance present the evidence of the delaying effect along a depth gradient, which corresponds to the water transfer during the drying process.

The movement of the evaporation front and the formation of the dry layer during the drying process were further discussed. Compared with the traditional point-based methods, the results of this study demonstrate the superiority of ERM to quantitatively estimate the soil water content dynamics, the soil moisture distribution in the near-surface zone, and the evaporation process with the identification of evaporation front in small-scale laboratory tests. Moreover, it highlights the potential of ERM to track soil water dynamics during frequent droughts happened in arid and semi-arid areas and further application in field investigation of soil water content variations driven by evapotranspiration, irrigation, precipitation, etc.

Funding information This work was supported by the National Key Research and Development Program of China (2019YFC1509902), the National Natural Science Foundation of China (Grant No. 41925012, 41902271, 41572246, 41772280), Natural Science Foundation of Jiangsu Province (BK20171228, BK20170394), and the Fundamental Research Funds for the Central Universities.

References

Ackerson JP, Morgan CLS, Everett ME, McInnes KJ (2014) The role of water content in electrical resistivity tomography of a vertisol. Soil Sci Soc Am J 78:1552–1562. https://doi.org/10.2136/sssaj2014.01.0032

Alamry AS, van der Meijde M, Noomen M, Addink EA, van Benthem R, de Jong SM (2017) Spatial and temporal monitoring of soil moisture using surface electrical resistivity tomography in Mediterranean soils. Catena 157:388–396. https://doi.org/10.1016/j.catena.2017.06.001

Aluwihare S, Watanabe K (2003) Measurement of evaporation on bare soil and estimating surface resistance. J Environ Eng 129:1157–1168. https://doi.org/10.1061/(ASCE)0733-9372(2003)129:12(1157)

An N, Hemmati S, Cui Y (2017) Numerical analysis of soil volumetric water content and temperature variations in an embankment due to soil-atmosphere interaction. Comput Geotech 83:40–51. https://doi.org/10.1016/j.compgeo.2016.10.010

An N, Hemmati S, Cui Y j, Tang C s (2018a) Numerical investigation of water evaporation from Fontainebleau sand in an environmental chamber. Eng Geol 234:55–64. https://doi.org/10.1016/j.enggeo.2018.01.005

An N, Tang CS, Xu SK, Gong XP, Shi B, Inyang HI (2018b) Effects of soil characteristics on moisture evaporation. Eng Geol 239:126–135. https://doi.org/10.1016/j.enggeo.2018.03.028

An N, Tang CS, Cheng Q, Wang DY, Shi B (2020) Application of electrical resistivity method in the characterization of 2D desiccation cracking process of clayey soil. Eng Geol 265. https://doi.org/10.1016/j.enggeo.2019.105416

Aoki T, Yokoi K (1997) Capacitance scaling system. IEEE Trans Instrum Meas 46:474–476. https://doi.org/10.1109/19.571889

Archie GE (1942) The electrical resistivity log as an aid in determining some reservoir characteristics. Trans AIME 146:54–62. https://doi.org/10.2118/942054-g

Beff L, Günther T, Vandoorne B, Couvreur V, Javaux M (2013) Three-dimensional monitoring of soil water content in a maize field using electrical resistivity tomography. Hydrol Earth Syst Sci 17:595–609. https://doi.org/10.5194/hess-17-595-2013

Benson AK, Payne KL, Stubben MA (1997) Mapping groundwater contamination using dc resistivity and VLF geophysical methods-a case study. Geophysics 62:80–86. https://doi.org/10.1190/1.1444148

Binley A, Kemna A (2005) Geophysical well logging: borehole geophysics for hydrogeological studies: principles and applications. In: Hydrogeophysics. Water and Science Technology Library, pp 129–156. https://doi.org/10.1007/1-4020-3102-5

Binley A, Henry-poulter S, Shaw B (1996) Examination of solute transport in an undisturbed soil column using electrical resistance tomography. Water Resour Res 32:763–769

Bittelli M (2011) Measuring soil water content: a review. Horttechnology 21:293–300. https://doi.org/10.21273/horttech.21.3.293

Brunet P, Clément R, Bouvier C (2010) Monitoring soil water content and deficit using electrical resistivity tomography (ERT) - a case study in the Cevennes area, France. J Hydrol 380:146–153. https://doi.org/10.1016/j.jhydrol.2009.10.032

Cahill AT, Parlange MB (1998) On water vapor transport in field soils. Water Resour Res 34:731–739. https://doi.org/10.1029/97WR03756

Calamita G, Brocca L, Perrone A, Piscitelli S, Lapenna V, Melone F, Moramarco T (2012) Electrical resistivity and TDR methods for soil moisture estimation in central Italy test-sites. J Hydrol 454–455:101–112. https://doi.org/10.1016/j.jhydrol.2012.06.001

Chambers JE, Gunn DA, Wilkinson PB, Ogilvy RD, Ghataora GS, Burrow MPN, Tilden Smith R (2008) Non-invasive time-lapse imaging of moisture content changes in earth embankments using electrical resistivity tomography (ERT). Adv. Transp. Geotech. - Proc. 1st Int. Conf. Transp. Geotech. 475–480. doi:https://doi.org/10.1201/9780203885949.pt6

Cheng Q, Tang CS, Zeng H, Zhu C, An N, Shi B (2020) Effects of microstructure on desiccation cracking of a compacted soil. Eng Geol 265. https://doi.org/10.1016/j.enggeo.2019.105418

Cui YJ, Lu YF, Delage P, Riffard M (2005) Field simulation of in situ water content and temperature changes due to ground–atmospheric interactions. Géotechnique 55:557–567. https://doi.org/10.1680/geot.2005.55.7.557

Cui YJ, Gao YB, Ferber V (2010) Simulating the water content and temperature changes in an experimental embankment using meteorological data. Eng Geol 114:456–471. https://doi.org/10.1016/j.enggeo.2010.06.006

Cui YJ, Ta AN, Hemmati S, Tang AM, Gatmiri B (2013) Experimental and numerical investigation of soil-atmosphere interaction. Eng Geol 165:20–28. https://doi.org/10.1016/j.enggeo.2012.03.018

Dahlin T (2001) The development of DC resistivity imaging techniques. Comput Geosci 27:1019–1029. https://doi.org/10.1016/S0098-3004(00)00160-6

Faměra M, Kotková K, Tůmová, Elznicová J, Matys Grygar T (2018) Pollution distribution in floodplain structure visualised by electrical resistivity imaging in the floodplain of the Litavka River, the Czech Republic. Catena 165:157–172. https://doi.org/10.1016/j.catena.2018.01.023

Frohlich RK, Parke CD (1989) The electrical resistivity of the vadose zone — field survey. Groundwater 27:524–530. https://doi.org/10.1111/j.1745-6584.1989.tb01973.x

Goyal VC, Gupta PK, Seth SM, Singh VN (1996) Estimation of temporal changes in soil moisture using resistivity method. Hydrol Process 10:1147–1154. https://doi.org/10.1002/(SICI)1099-1085(199609)10:9<1147::AID-HYP366>3.0.CO;2-S

Gunn DA, Chambers JE, Uhlemann S, Wilkinson PB, Meldrum PI, Dijkstra TA, Haslam E, Kirkham M, Wragg J, Holyoake S, Hughes PN, Hen-Jones R, Glendinning S (2015) Moisture monitoring in clay embankments using electrical resistivity tomography. Constr Build Mater 92:82–94. https://doi.org/10.1016/j.conbuildmat.2014.06.007

Gupta SC, Hans RJ (1972) Influence of water content on electrical conductivity of the soil. Soil Sci Soc Am Proc 36:855–857. https://doi.org/10.2136/sssaj1972.03615995003600060011x

Hakhamaneshi M, Black JA, Cargill A, Cox CM, Elmrom T (2016) Development and calibration of a sand pluviation device for preparation of model sand bed for centrifuge tests. In: Proceedings of the 3rd European Conference on Physical Modelling in Geotechnics (EUROFUGUE). Sheffield pp 73–79

Hayley K, Bentley LR, Gharibi M, Nightingale M (2007) Low temperature dependence of electrical resistivity: implications for near surface geophysical monitoring. Geophys Res Lett 34:1–5. https://doi.org/10.1029/2007GL031124

Jones G, Sentenac P, Zielinski M (2014) Desiccation cracking detection using 2-D and 3-D electrical resistivity tomography: validation on a flood embankment. J Appl Geophys 106:196–211. https://doi.org/10.1016/j.jappgeo.2014.04.018

Kalinski RJ, Kelly WE, Bogardi I, Pesti G (1993) Electrical resistivity measurements to estimate travel times through unsaturated ground water protective layers. J Appl Geophys 30:161–173. https://doi.org/10.1016/0926-9851(93)90024-S

Kearey P, Brooks M, Hill I (2002) An introduction to geophysical exploration. Blackwell Science, Hoboken

Keller G, Frischknecht F (1966) Electrical methods in geophysical prospecting. In: Int. Ser. Monogr. Electromagn. Waves. Pergamon, Oxford, N. Y

Kondo J, Saigusa N, Sato T (1990) A parameterization of evaporation from bare soil surfaces. J Appl Meteorol 29:385–389

Lal R, Shukla MK (2004) Principles of soil physics. Marcel Dekker, New York. https://doi.org/10.1017/CBO9781107415324.004

Li HD, Tang CS, Cheng Q, Li SJ, Gong XP, Shi B (2019) Tensile strength of clayey soil and the strain analysis based on image processing techniques. Eng Geol 253:137–148. https://doi.org/10.1016/j.enggeo.2019.03.017

Maeda K (1974) An automatic, precision 1-MHz digital LCR meter. HP J. March, 1–9

Martínez-Pagán P, Cano ÁF, Da Silva GRR, Olivares AB (2010) 2-D electrical resistivity imaging to assess slurry pond subsoil pollution in the southeastern region of Murcia, Spain. J Environ Eng Geophys 15:29–47. https://doi.org/10.2113/JEEG15.1.29

McCarter WJ (1984) The electrical resistivity characteristics of compacted clays. Geotechnique 34:263–267. https://doi.org/10.1680/geot.1984.34.2.263

Miura S, Toki S (1982) A sample preparation method and its effect on static and cyclic deformation-strength properties of sand. Chem Pharm Bull 22:61–77

Mohamed AA, Sasaki T, Watanabe K (2000) Solute transport through unsaturated soil due to evaporation. J Environ Eng 126:842–848. https://doi.org/10.1061/(ASCE)0733-9372(2000)126:9(842)

Negri S, Leucci G, Mazzone F (2008) High resolution 3D ERT to help GPR data interpretation for researching archaeological items in a geologically complex subsurface. J Appl Geophys 65:111–120. https://doi.org/10.1016/j.jappgeo.2008.06.004

Newson TA, Fahey M (2003) Measurement of evaporation from saline tailings storages. Eng Geol 70:217–233. https://doi.org/10.1016/S0013-7952(03)00091-7

Penman HL (1948) Natural evaporation from open water, hare soil and grass. Proc R Soc Lond A Math Phys Sci 193:120–145. https://doi.org/10.1098/rspa.1948.0037

Pitzer KS (1982) Self-ionization of water at high temperature and the thermodynamic properties of the ions. J Phys Chem 86:4704–4708. https://doi.org/10.1021/j100221a013

Qiu GY, Yano T, Momii K (1998) An improved methodology to measure evaporation from bare soil based on comparison of surface temperature with a dry soil surface. J Hydrol 210:93–105. https://doi.org/10.1016/S0022-1694(98)00174-7

Reichling K, Raupach M, Klitzsch N (2015) Determination of the distribution of electrical resistivity in reinforced concrete structures using electrical resistivity tomography. Mater Corros 66:763–771. https://doi.org/10.1002/maco.201407763

Rhoades JD, Raats PAC, Prather RJ (1976) Effects of liquid-phase electrical conductivity, water content, and surface conductivity on bulk soil electrical conductivity. Soil Sci Soc Am J 40:651. https://doi.org/10.2136/sssaj1976.03615995004000050017x

Rhoades JD, Kaddah M, Halvorson AD, Prather RJ (1977) Establishing soil electrical conductivity-salinity calibrations using four-electrode cells containing undisturbed soil cores. Soil Sci 123:137–141

Rhoades JD, Shouse PJ, Alves WJ, Manteghi NA, Lesch SM (1990) Determining soil salinity from soil electrical conductivity using different models and estimates. Soil Sci Soc Am J 54:46–54. https://doi.org/10.2136/sssaj1990.03615995005400010007x

Rothe A, Weis W, Kreutzer K, Matthies D, Hess U, Ansorge B (1997) Changes in soil structure caused by the installation of time domain reflectometry probes and their influence on the measurement of soil moisture. Water Resour Res 33:1585–1593. https://doi.org/10.1029/97WR00677

Saito H, Simunek J, Mohanty BP (2006) Numerical analysis of coupled water, vapor, and heat transport in the vadose zone. Vadose Zone J 5:784–800. https://doi.org/10.2136/vzj2006.0007

Samouëlian A, Cousin I, Tabbagh A, Bruand A, Richard G (2005) Electrical resistivity survey in soil science: a review. Soil Tillage Res 83:173–193. https://doi.org/10.1016/j.still.2004.10.004

Samson G, Deby F, Garciaz JL, Perrin JL (2018) A new methodology for concrete resistivity assessment using the instantaneous polarization response of its metal reinforcement framework. Constr Build Mater 187:531–544. https://doi.org/10.1016/j.conbuildmat.2018.07.158

Scollar I, Tabbagh A, Hesse A, Herzog I (1990) Archaeological prospecting and remote sensing

Shahraeeni E, Lehmann P, Or D (2012) Coupling of evaporative fluxes from drying porous surfaces with air boundary layer: characteristics of evaporation from discrete pores. Water Resour Res 48:1–15. https://doi.org/10.1029/2012WR011857

Shimojima E, Yoshioka R, Tamagawa I (1996) Salinization owing to evaporation from bare-soil surfaces and its influences on the evaporation. J Hydrol 178:109–136. https://doi.org/10.1016/0022-1694(95)02826-9

Shokri N, Lehmann P, Vontobel P, Or D (2008) Drying front and water content dynamics during evaporation from sand delineated by neutron radiography. Water Resour Res 44:1–11. https://doi.org/10.1029/2007WR006385

Singh VP, Xu CY (1997) Evaluation and generalization of 13 mass-transfer equations for determining free water evaporation. Hydrol Process 11:311–323. https://doi.org/10.1002/(SICI)1099-1085(19970315)11:3<311::AID-HYP446>3.3.CO;2-P

Smethurst J, Clarke D, Powrie W (2012) Factors controlling the seasonal variation in soil water content and pore water pressures within a lightly vegetated clay slope. Géotechnique 62:429–446. https://doi.org/10.1680/geot.10.P.097

Song WK, Cui YJ, Tang AM, Ding WQ, Tran TD (2014) Experimental study on water evaporation from sand using environmental chamber. Can Geotech J 51:115–128. https://doi.org/10.1139/cgj-2013-0155

Tang CS, Cui YJ, Shi B, Tang AM, Liu C (2011a) Desiccation and cracking behaviour of clay layer from slurry state under wetting-drying cycles. Geoderma 166:111–118. https://doi.org/10.1016/j.geoderma.2011.07.018

Tang CS, Shi B, Gu K (2011b) Experimental investigation on soil water evaporation process during drying (in Chinese). J Eng Geol 19:1–7

Tang CS, Wang DY, Zhu C, Zhou QY, Xu SK, Shi B (2018) Characterizing drying-induced clayey soil desiccation cracking process using electrical resistivity method. Appl Clay Sci 152:101–112. https://doi.org/10.1016/j.clay.2017.11.001

Tang CS, Zhu C, Leng T, Shi B, Cheng Q, Zeng H (2019) Three-dimensional characterization of desiccation cracking behavior of compacted clayey soil using X-ray computed tomography. Eng Geol 255:1–10. https://doi.org/10.1016/j.enggeo.2019.04.014

Tarboton DG (2003) Rainfall-runoff processes. Utah state university, Logan

Teng J, Yasufuku N (2015) Evaluation of in-situ variation of water content and temperature due to soil-atmosphere interaction by a lysimeter test. Memoirs of the Faculty of Engineering, Kyushu University 74:53–67

Teng J, Yasufuku N, Liu Q, Liu S (2014) Experimental evaluation and parameterization of evaporation from soil surface. Nat Hazards 73:1405–1418. https://doi.org/10.1007/s11069-014-1138-z

Toll DG, Lourenço SDN, Mendes J (2013) Advances in suction measurements using high suction tensiometers. Eng Geol 165:29–37. https://doi.org/10.1016/j.enggeo.2012.04.013

Tollenaar RN, van Paassen LA, Jommi C (2018) Small-scale evaporation tests on clay: influence of drying rate on clayey soil layer. Can Geotech J 55:437–445. https://doi.org/10.1139/cgj-2017-0061

Tonkov N, Loke MH (2006) A resistivity survey of a burial mound in the "Valley of the Thracian Kings". Archaeol Prospect 13:129–136. https://doi.org/10.1002/arp.273

Tso CHM, Kuras O, Wilkinson PB, Uhlemann S, Chambers JE, Meldrum PI, Graham J, Sherlock EF, Binley A (2017) Improved characterisation and modelling of measurement errors in electrical resistivity tomography (ERT) surveys. J Appl Geophys 146:103–119. https://doi.org/10.1016/j.jappgeo.2017.09.009

Vaid Y, Negussey D (1998) Preparation of reconstituted sand specimens. Advanced triaxial testing of soil and rock. ASTM International: 405–417. https://doi.org/10.1520/stp29090s

van de Griend AA, Owe M (1994) Bare soil surface resistance to evaporation by vapor diffusion under semiarid conditions. Water Resour Res 30:181–188. https://doi.org/10.1029/93WR02747

Wang G, Zhou Q, Wu S, Ling C, Yang X, Lei M (2012) An in-situ experimental study of fractures network identification within bedrock by high-density electrical resistivity tomography. Geological Review 58:165–174 (in Chinese)

Wang DY, Tang CS, Cui YJ, Shi B, Li J (2016) Effects of wetting-drying cycles on soil strength profile of a silty clay in micro-penetrometer tests. Eng Geol 206:60–70. https://doi.org/10.1016/j.enggeo.2016.04.005

Wang LL, Tang CS, Shi B, Cui YJ, Zhang GQ, Hilary I (2018) Nucleation and propagation mechanisms of soil desiccation cracks. Eng Geol 238:27–35. https://doi.org/10.1016/j.enggeo.2018.03.004

Wilson GW, Fredlund DG, Barbour SL (1994) Coupled soil-atmosphere modelling for soil evaporation. Can Geotech J 31:151–161. https://doi.org/10.1139/t94-021

Wilson GW, Fredlund DG, Barbour SL (1997) The effect of soil suction on evaporative fluxes from soil surfaces. Can Geotech J 34:145–155. https://doi.org/10.1139/t98-034

Wyseure GCL, Mojid MA, Malik MA (1997) Measurement of volumetric water content by TDR in saline soils. Eur J Soil Sci 48:347–354. https://doi.org/10.1111/j.1365-2389.1997.tb00555.x

Xue Z, Akae T (2012) Maximum surface temperature model to evaluate evaporation from a saline soil in arid area. Paddy Water Environ 10:153–159. https://doi.org/10.1007/s10333-011-0286-y

Yamanaka T, Takeda A, Sugita F (1997) A modified surface-resistance approach for representing bare-soil evaporation: wind tunnel experiments under various atmospheric conditions. Water Resour Res 33:2117–2128. https://doi.org/10.1029/97WR01639

Yanful EK, Choo LP (1997) Measurement of evaporative fluxes from candidate cover soils. Can Geotech J 34:447–459. https://doi.org/10.1139/t97-002

Zeng LL, Hong ZS, Cui YJ (2015) On the volumetric strain–time curve patterns of dredged clays during primary consolidation. Géotechnique 65 (12):1023-1028

Zeng H, Tang C s, Cheng Q, Inyang HI, Rong D z, Lin L, Shi B (2019) Coupling effects of interfacial friction and layer thickness on soil desiccation cracking behavior. Eng Geol 260:105220. https://doi.org/10.1016/j.enggeo.2019.105220

Zha FS, Liu SY, Du YJ, Cui KR (2007) The electrical resistivity characteristics of unsaturated clayey soil (in Chinese). Rock Soil Mech 28:1671–1676

Zhou QY (2007) A sensitivity analysis of DC resistivity prospecting on finite, homogeneous blocks and columns. Geophysics 72:F237–F247. https://doi.org/10.1190/1.2770537

Zhou QY, Shimada J, Sato A (2001) Three-dimensional spatial and temporal monitoring of soil water content using electrical tomography. Water Resour Res 37:273–285. https://doi.org/10.1029/2000WR900284

Zhu JJ, Kang HZ, Gonda Y (2007) Application of Wenner configuration to estimate soil water content in pine plantations on sandy land. Pedosphere 17:801–812. https://doi.org/10.1016/S1002-0160(07)60096-4